Available online www.jsaer.com

Journal of Scientific and Engineering Research, 2023, 10(5):249-260

Research Article

ISSN: 2394-2630
CODEN(USA): JSERBR

Series Resistance Effect on the Performance of a Photovoltaic Cell

E.M. Keita*, F. Mbaye, S. Seck, M.S. Mane, C. Sene, B. Mbow

Laboratoire des Semiconducteurs et d'Energie Solaire, Département de Physique, Faculté des Sciences et Techniques, Université Cheikh Anta Diop, Dakar, Sénégal
Corresponding author: elouazy@hotmail.fr

Abstract In this paper we study the influence of series resistance on the performance of a solar cell. This study is applied to the heterostructure type n^+n/pp^+ based on chalcopyrite materials type $CuInS_2$ and $CuInSe_2$ and is modeled in two and three-dimensional representations. We consider the single diode model, this model takes into account the presence of parasitic resistances (series and shunt resistances) which reduce the performance of the solar cell. We highlight the influence of the series resistance on the evolutions of the current - voltage and power - voltage characteristics, its influence on the electrical parameters such as the open-circuit voltage (v_{oc}),the short circuit current (J_{sc}), the fill factor (FF) and the efficiency (η_c) is also studied. The determination of certain electrical parameters of a real solar cell is quite complex and is the subject of several calculation models, to determine these parameters we have used particularly a numerical method and precisely the secant method. We consedered series resistance values ranging from 0 $\Omega.cm^2$ to 30 $\Omega.cm^2$. The results obtained show that the increase in the series resistance reduces the performance of the solar cell, it modifies the evolution of the current-voltage and power-voltage characteristics. The effect of the series resistance is visible on the current-voltage curve by the appearance of a slope in the vicinity of the open-circuit voltage. According to the values of the parameters considered in this paper, the power obtained varies between 11 $mW.cm^{-2}$ and 4.4 $mW.cm^{-2}$. Parameters such as the fill factor, the short-circuit current and the efficiency decrease when the series resistance increases. Thus the fill factor varies between 0.8 and 0.2, the short-circuit current between 17 $mA.cm^{-2}$ and 14 $mA.cm^{-2}$ and the efficiency between 6% and 12% (for shunt resistance greater than 150 $\Omega.cm^2$). The open-circuit voltage remains independent of the series resistance.

Keywords Series resistance, Electrical parameters, Solar cell performance

Introduction

The performance of a photovoltaic cell depends on its electrical parameters (short-circuit current, open-circuit voltage, maximum power point, fill factor). Several electrical models are used to model the operation of a solar cell. Among these models we can cite the double diode model (comprising 7 parameters), the single diode model (comprising 5 parameters) [1-4] and the ideal model. The ideal model is used in the absence of parasitic resistances whereas the models with single diode and double diode take into account the presence of series and shunt resistances. The presence of series resistance is due to electrical voltage drops in the different layers of the solar cell, the presence of shunt resistance is due to current leakage in the different layers due generally by dislocations and device faults. The study of the series resistance on the performance of the photovoltaic cell first requires the determination of the electrical parameters. A real solar cell (presence of parasitic resistance) is generally described by an implicit relation between the voltage and the current, thus the access to the electric parameters calls upon techniques of approximate calculation. Several formulations are used for the determination of the electrical parameters [5-10], we can quote the function of Lambert, curve-fitting method, iterative 5-point method, analytical 5-point method, Newton's method, genetic algorithm [11-18]. To have access to these parameters we have particularly developed in previous studies a numerical method called the secant method [18-20]. The results obtained are applied to the solar cell based on $CuInS_2$ and $CuInSe_2$ chalcopyrite materials according to the model n^+n/pp^+ type $ZnO(n^+)/CdS(n)/CuInS_2(p)/CuInSe_2(p^+)$. $CuInS_2$ and

$CuInSe_2$ are direct gap materials with photovoltaic properties in the range from near infrared to visible. The study of the spectral response of these cells and the influence of geometric and electrical parameters are widely developed in our previous studies [21-22].

Materials and Methods

Photocurrent density supplied by the solar cell

In this work we consider the 4-layer model $ZnO(n^+)/CdS(n)/CuInS_2(p)/CuInSe_2(p^+)$ represented in figure 1 by . its energy band diagram [21]. The photocurrent generated by the device is due to the generated minority carriers of charges. The calculation methods of the photocurrent density are largely done by our previous studies [21-23] and are indicated in the appendix.

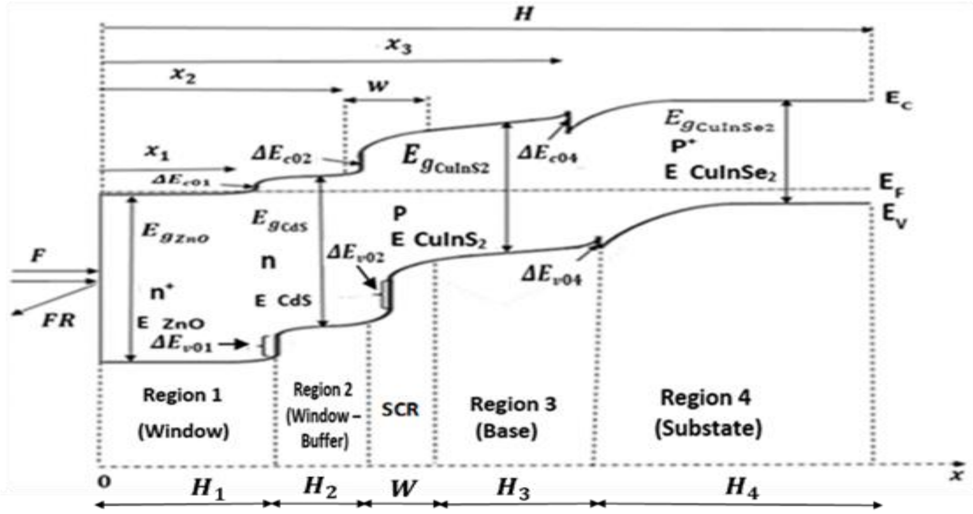

Figure 1: Energy band diagram of the structure $ZnO(n^+)/CdS(n)/ CuInS_2(p)/CuInSe_2(p^+)$ [21]

For the model n^+n/pp^+, in region 1 doped n^+, the photocurrent is essentially due to the generated holes, the contribution to the photocurrent by this region can be written as [21-23]:

$$J_{p_1} = \frac{q\alpha_1 F(1-R)L_{p_1}}{(\alpha_1^2 {L_{p_1}}^2-1)\left[\frac{Sp_2 Lp_2}{Dp_2}sh\left(\frac{H_2}{Lp_2}\right)+ch\left(\frac{H_2}{Lp_2}\right)\right]} \times \left\{\frac{\left(\frac{Sp_1 Lp_1}{Dp_1}+\alpha_1 L_{p_1}\right)- e^{-\alpha_1 H_1}\left[\frac{Sp_1 Lp_1}{Dp_1}ch\left(\frac{H_1}{Lp_1}\right)+sh\left(\frac{H_1}{Lp_1}\right)\right]}{\frac{Sp_1 Lp_1}{Dp_1}sh\left(\frac{H_1}{Lp_1}\right)+ch\left(\frac{H_1}{Lp_1}\right)} - \alpha_1 L_{p_1} e^{-\alpha_1 H_1}\right\} \quad (1)$$

In region 2 doped n, the photocurrent is also due to the generated holes, its contribution to the photocurrent is given by :

$$J_{p_2} = \frac{q\alpha_2 F(1-R)L_{p_2} e^{-\alpha_1 H_1}}{({\alpha_2}^2 {L_{p_2}}^2 -1)}\left\{\frac{\left(\frac{Sp_2 Lp_2}{Dp_2}+\alpha_2 L_{p_2}\right)}{\frac{Sp_2 Lp_2}{Dp_2}sh\left(\frac{H_2}{Lp_2}\right)+ch\left(\frac{H_2}{Lp_2}\right)} - \frac{e^{-\alpha_2 H_2}\left[\frac{Sp_2 Lp_2}{Dp_2}ch\left(\frac{H_2}{Lp_2}\right)+sh\left(\frac{H_2}{Lp_2}\right)\right]}{\frac{Sp_2 Lp_2}{Dp_2}sh\left(\frac{H_2}{Lp_2}\right)+ch\left(\frac{H_2}{Lp_2}\right)} -\alpha_2 L_{p_2} e^{-\alpha_2 H_2}\right\} \quad (2)$$

The hole photocurrent due to the contribution of regions 1 and 2 is written as:

$$J_{p_{1-2}} = J_{p_1} + J_{p_2} \quad (3)$$

In region 3 doped p, the photocurrent is due to the generated electrons. The contribution of this region to the photocurrent is also given by previous studies [21-23], it is written as:

$$J_{n_3} = -\frac{q\,\alpha_3\,L_{n_3} F(1-R)\,e^{[(\alpha_2-\alpha_1)H_1]}\,e^{[(\alpha_3-\alpha_2)(H_1+H_2+w_1)]}}{({\alpha_3}^2 {L_{n_3}}^2 -1)} \times \left[\frac{\left(\alpha_3 L_{n_3} - \frac{Sn_3 Ln_3}{Dn_3}\right) e^{-\alpha_3(H-H_4)}}{\frac{Sn_3 Ln_3}{Dn_3}sh\left[\frac{H_3}{Ln_3}\right]+ch\left[\frac{H_3}{Ln_3}\right]} + \right.$$

$$\left.\frac{e^{-\alpha_3(H_1+H_2+w)}\left[\frac{Sn_3 Ln_3}{Dn_3}\cdot \mathrm{ch}\left(\frac{H_3}{Ln_3}\right)+\mathrm{sh}\left(\frac{H_3}{Ln_3}\right)\right]}{\frac{Sn_3 Ln_3}{Dn_3}sh\left[\frac{H_3}{Ln_3}\right]+ch\left[\frac{H_3}{Ln_3}\right]} - \alpha_3 L_{n_3} e^{-\alpha_3(H_1+H_2+w)}\right] \quad (4)$$

In region 4 doped p+, the photocurrent is also due to the photo-created electrons, it expression is given by :

$$J_{n_4} = -\frac{q\,\alpha_4\,L_{n_4}F(1-R)\,e^{[(\alpha_2-\alpha_1)H_1]}\,e^{[(\alpha_3-\alpha_2)(H_1+H_2+w_1)]}}{(\alpha_4{}^2L_{n_4}{}^2-1)\left\{\frac{S_{n_3}L_{n_3}}{D_{n_3}}sh\left[\frac{H_3}{L_{n_3}}\right]+ch\left[\frac{H_3}{L_{n_3}}\right]\right\}} \times e^{[(\alpha_4-\alpha_3)(H-H_4)]} \times \left[\frac{\left(\alpha_4 L_{n_4}-\frac{S_{n_4}L_{n_4}}{D_{n_4}}\right)e^{-\alpha_4 H}}{\frac{S_{n_4}L_{n_4}}{D_{n_4}}sh\left(\frac{H_4}{L_{n_4}}\right)+ch\left(\frac{H_4}{L_{n_4}}\right)} + \frac{e^{-\alpha_4(H-H_4)}\left[\frac{S_{n_4}L_{n_4}}{D_{n_4}}\cdot \mathrm{ch}\left(\frac{H_4}{L_{n_4}}\right)+\mathrm{sh}\left(\frac{H_4}{L_{n_4}}\right)\right]}{\frac{S_{n_4}L_{n_4}}{D_{n_4}}sh\left(\frac{H_4}{L_{n_4}}\right)+ch\left(\frac{H_4}{L_{n_4}}\right)} - \alpha_4 L_{n_4}e^{-\alpha_4(H-H_4)}\right] \quad (5)$$

The electron photocurrent due to the contribution of regions 3 and 4 is written as:

$$J_{n_{3-4}} = J_{n_3} + J_{n_4} \quad (6)$$

In the space charge region (SCR), the recombination phenomena are neglected, its contribution to the photocurrent is given by [21]:

$$J_{SCR} = -qF(1-R)e^{-\alpha_1 H_1}\{e^{-\alpha_2 H_2}\times[e^{-\alpha_2 w_1}-1]+e^{-\alpha_2(H_2+w_1)}\times[e^{-\alpha_3 w_2}-1]\} \quad (7)$$

The total photocurrent is the sum of the contributions of the different regions, it is given by:

$$J_{np} = J_{p_{1-2}} + J_{n_{3-4}} + J_{SCR} \quad (8)$$

The total internal quantum efficiency or spectral response S_{re} is written as:

$$S_{re} = \frac{J_{np}}{qF(1-R)} \quad (9)$$

The external quantum efficiency EQE is written as:

$$IQE = S_{re}(1-R) \quad (10)$$

α_i represents the absorption coefficient of the layer i, L_{p_i} and L_{n_i} represent respectively the diffusion length of holes and electrons in region i, D_{p_i} and D_{n_i} the diffusion coefficient of charge carriers, S_{p_i} and S_{n_i} recombination velocities at the surface and at the interface, F is the photon flux, H_i is the thickness of the layer i, R is the reflection coefficient of the frontal layer and q is the elementary charge. The absorption coefficient (αi) and the photon flux (F) depend on the photon energy.

The current density generated by the illumination J_{ph} is determine by numerical method, it is given by [23] :

$$J_{ph} = \int_1^4 qF(1-R)S_{re}\,dE \approx \frac{\delta E}{2}\left[J_{np}(E_1)+J_{np}(E_{m+1})+2\sum_{i=2}^{m}J_{np}(E_i)\right] \quad (11)$$

With: $E \in [1\,eV, 4\,eV]$; $E_1 = 1\,eV$; $E_{m+1} = 4\,eV$; $\delta E = \frac{E_{m+1}-E_1}{m}\,(eV)$; $m = 100$

$E_{i+1} = E_1 + i\cdot\delta E\,(eV)$ with: $i : 1 \ldots m$

Single diode model and electrical parameters

In this paper, to study the electrical parameters we consider the single diode model which is the most used in the literature. The single diode model takes into account the presence of series and shunt resistances, it is described by equations (12) and is symbolized by figure 2. The method of determining the electrical parameters has already been done by our previous studies [18-19].

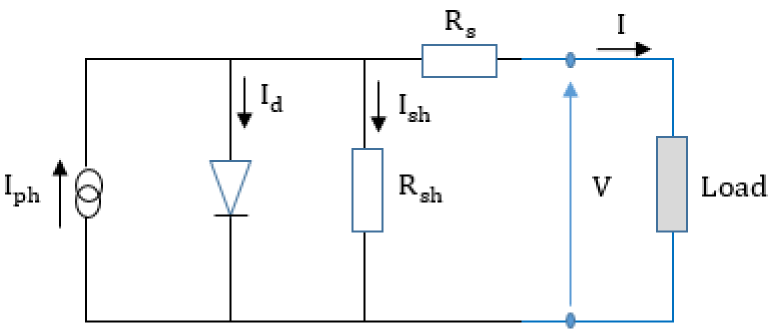

Figure 2: Equivalent electrical diagram of a single diode model.

$$J = J_{ph} - J_0 \left(e^{\frac{q\,(V+R_S J)}{\eta KT}} - 1 \right) - \frac{V+R_S J}{R_{sh}} \quad (12)$$

J_0 is the saturation current density, K is the Boltzmann constant, η is the ideality factor, T is the temperature, q is the elementary charge, J_{ph} is the photo-generated current density due to the illumination and is given by equation (11). This model contains 5 physical parameters to be determined J_0, R_{sh}, R_s, η, J_{ph},.

The relation between the current I (A) delivered by the solar cell and the current density J (A.cm^{-2}) is written as:

$$I = J \times A_s \quad (13)$$

A_s is the active surface of the solar cell (m^2).

The short-circuit current density J_{sc} is obtained when the voltage V is zero in equation (12), it is given by the implicit relation:

$$J_{sc} = \frac{\eta KT}{q\,R_S} \cdot \ln\left(\frac{J_{ph}}{J_0} - \frac{J_{sc}}{J_0} - \frac{R_S\,J_{sc}}{R_{sh}\,J_0} + 1 \right) \quad (14)$$

The short-circuit current density depends on the shunt and series resistances.

The open-circuit voltage V_{oc} is obtained when the current density J is zero in equation (12), it is given by the implicit relation:

$$V_{oc} = \frac{\eta KT}{q} \ln\left(\frac{J_{ph}}{J_0} - \frac{V_{oc}}{R_{sh}\,J_0} + 1 \right) \quad (15)$$

It does not depend on the series resistance, it only depends on the shunt resistance.

The electrical power density is defined by the relation:

$$P = \left[J_{ph} - J_0 \left(e^{\frac{q\,(V+R_S J)}{\eta KT}} - 1 \right) - \frac{V+R_S J}{R_{sh}} \right] \cdot V \quad (16)$$

At the maximum power density point, we can write:

$$\frac{\partial P}{\partial V} = 0 \quad (17)$$

So we can write [19]:

$$J = -V \frac{\partial J}{\partial V} \quad (18)$$

At the maximum power density point, we obtain the implicit relation:

$$J - \frac{\frac{q\,V\,J_0}{\eta KT} e^{\frac{q\,(V+R_S J)}{\eta KT}} + \frac{V}{R_{sh}}}{1 + \frac{q\,J_0\,R_S}{\eta KT} e^{\frac{q\,(V+R_S J)}{\eta KT}} + \frac{R_S}{R_{sh}}} = 0 \quad (19)$$

To determine the current density J_m and the voltage V_m at the maximum power density point P_m, the solution of relation (19) must verify equation (12) which models the operation of the solar cell. Approximate solving techniques are used to solve the various implicit equations.

The fill factor FF is defined by the relation:

$$FF = \frac{P_m}{J_{sc} \cdot V_{oc}} \quad (20)$$

The electrical conversion efficiency η_C of the solar cell is given by the relation:

$$\eta_C = \frac{FF \times V_{oc} \times J_{sc}}{S_r} \quad (21)$$

S_r is the solar radiation (W/m^2).

The results obtained are applied to the heterojunction ZnO(n$^+$)/CdS(n)/$CuInS_2$(p)/ $CuInSe_2$(p$^+$) to evaluate the performance and study the effects of the series resistance on the electrical parameters.

Results & Discussion

The values of the standard parameters used for the modeling are indicated in the following table 1.

Table 1: Physical standard parameters considered.

Parameters	
Region 1	Region 3
$H_1 = 0.3$ µm	$H_3 = 1$ µm
$Lp_1 = 0.3$ µm	$Ln_3 = 3$ µm
$Sp_1 = 2.10^7$ cm.s^{-1}	$Sn_3 = 2.10^5$ cm.s^{-1}
$Dp_1 = 0.51$ cm^2.s^{-1}	$Dn_3 = 5.13$ cm^2.s^{-1}
Region 2	Region 4
$H_2 = 0.1$ µm	$H_4 = 98.5$ µm
$Lp_2 = 0.4$ µm	$Ln_4 = 1$ µm
$Sp_2 = 2.10^5$ cm.s^{-1}	$Sn_4 = 2.10^7$ cm.s^{-1}
$Dp_2 = 0.64$ cm^2.s^{-1}	$Dn_4 = 10.27$ cm^2.s^{-1}
Space charge region	
$W_1 = 0.02$ µm	$W_2 = 0.08$ µm

Based on previous studies [18-19], the saturation current density J_0 is estimated at $J_0 = 4.117 \times 10^{-8}\, mA \cdot cm^{-2}$ for a junction CdS(n)/CuInS$_2$(p). Figure 3 shows the external quantum efficiency (equation 10) versus photon energy, it is represented in bar histogram. Figure 3 also shows the resulting photocurrent density of minority carriers J_{np} (equation 8) versus the photon energy under AM1.5 solar spectrum [19, 24]. The photo-generated current density due to the illumination Jph delivered by the solar cell which corresponds to the response of the device in figure 3 is calculated using equation (11) and table 1, it is estimated at 17 $mA \cdot cm^{-2}$. For this paper we choose the ideality factor η = 1.5 [25].

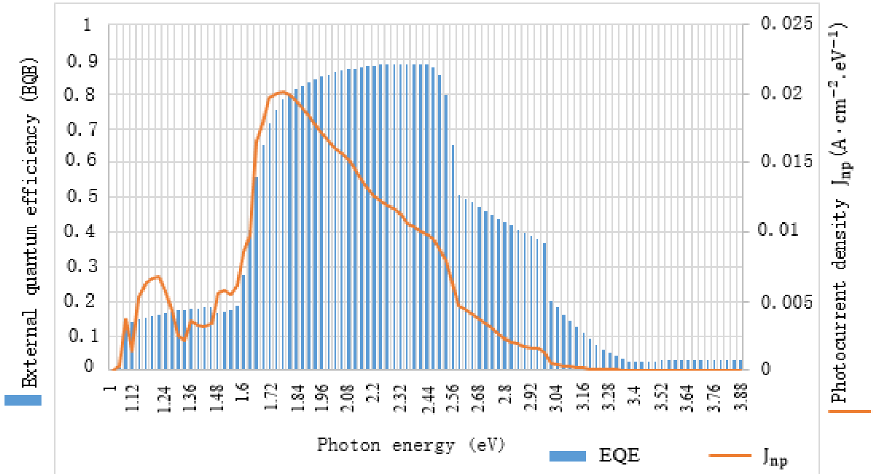

Figure 3: Bar histogram of the external quantum efficiency and photocurrent density under AM1.5 solar spectrum vs. photon energy

Effect of series resistance on the current-voltage J(V) characteristic

The effect of series resistance is highlighted in figures 4. We study the evolutions of the current density J and the electrical power P versus the bias voltage for different values of the series resistance R_S ranging between 0 Ω.cm^2 and 30 Ω.cm^2. The shunt resistance R_{SH} is fixed at 600 Ω.cm^2. The effect of the series resistance can be easily perceived on the characteristic current-voltage J(V) by the appearance of a slope S near the open-circuit voltage V_{oc} with $S = -\frac{1}{R_S}$ (figures 4-b, 4-c and 4-d), it describes a linear line given by the equation:

$$J\,(V) = -\frac{V}{R_S} + \frac{V_{OC}}{R_S} \tag{22}$$

V_{oc} is evaluated at 0.76 V. In this linear part described by equation (22), the solar cell can be assimilated to a voltage generator whose equivalent electrical diagram is shown in figure 5.

In figures 6 we represent the evolution of the current density J (figure 6-a) and the electrical power P (figure 6-b) versus the bias voltage for different values of the series resistance between 0 $\Omega.cm^2$ and 30 $\Omega.cm^2$. The shunt resistance is fixed at 600 $\Omega.cm^2$.

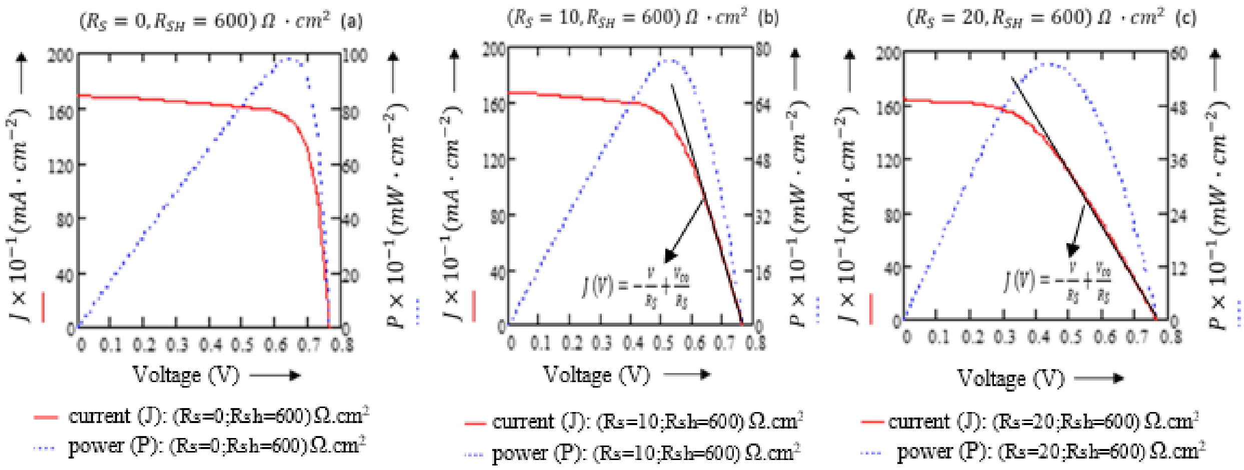

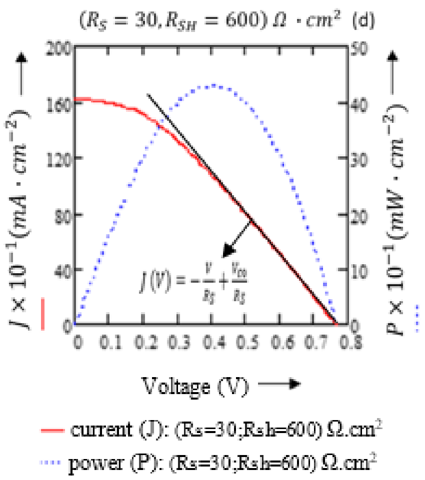

Figure 4: Evolution of current density J and electrical power P versus bias voltage V for various values of series resistance
a) $R_S = 0\ \Omega.cm^2$ *; b)* $R_S = 10\ \Omega.cm^2$ *;c)* $R_S = 20\ \Omega.cm^2$*; d)* $R_S = 30\ \Omega.cm^2$
$(J_0 = 4.117 \cdot 10^{-8}\ mA \cdot cm^{-2}; J_{ph} = 17 mA \cdot cm^{-2}; R_{SH} = 600\ \Omega.cm^2; \eta = 1.5)$

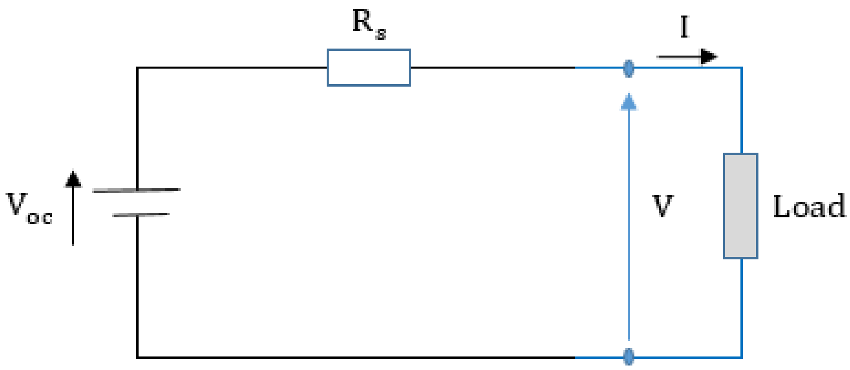

Figure 5: Equivalent electrical diagram of a solar cell in presence of high value of series resistance

In figure 6-a, we observe that the open-circuit voltage V_{oc} is independent of the series resistance. A slight decrease of the short-circuit current J_{sc} is observed for high values of R_S (for R_S=30 Ω.cm^2), J_{sc} varies from 17 mA.cm^{-2} to 16 mA.cm^{-2}. Also we notice that an increase of the slope S improves the performance of the solar cell. In figure 6-b, we represent the evolution of the electrical power density, it is all the greater as the series resistance is low. The ideal maximum power density obtained with $R_S = 0\,\Omega.\text{cm}^2$ and $R_{Sh} = \infty\,\Omega.\text{cm}^2$ is slightly less than 11 mW .cm^{-2}. For series resistance values ranging between 0 Ω.cm^2 and 30 Ω.cm^2 and R_{SH} > 600 Ω.cm^2 the maximum power varies between 4.4 mW.cm^{-2} and 11 mW.cm^{-2} for the considered structure $ZnO(n^+)/CdS(n)/ CuInS_2(p)/CuInSe_2(p^+)$.

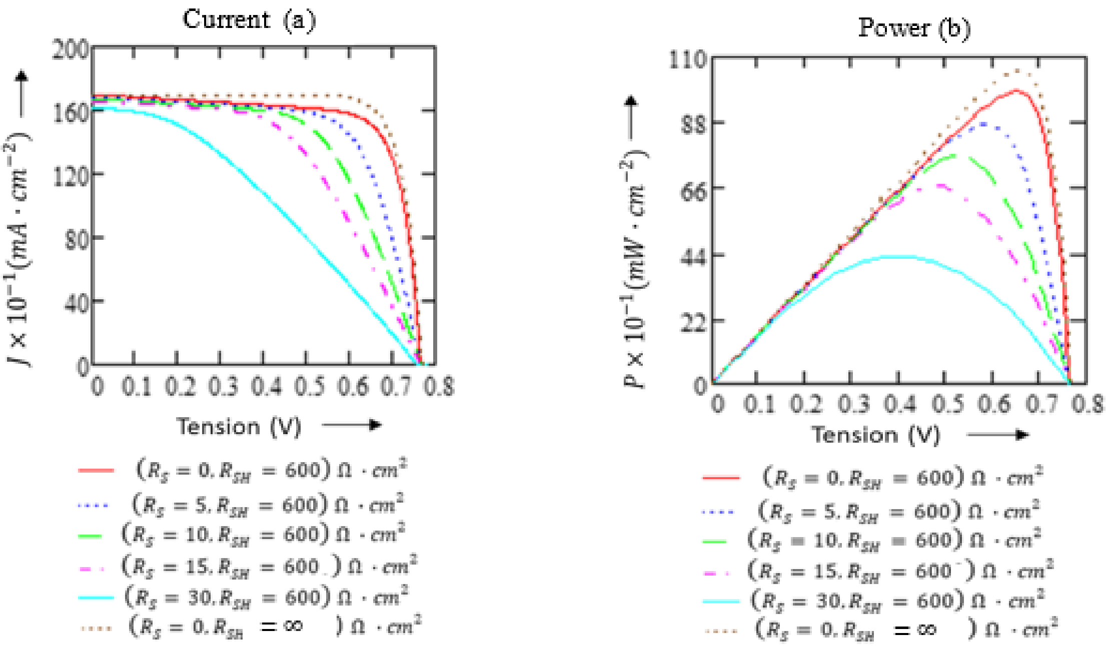

Figure 6: (a) Evolution of current density J versus bias voltage V for various values of series resistance ($R_S = 0\,\Omega.cm^2 - 30\,\Omega.cm^2$) and (b) Evolution of electrical power density P versus bias voltage V for various values of series resistance ($R_S = 0\,\Omega.cm^2 - 30\,\Omega.cm^2$)
($J_0 = 4.117 \cdot 10^{-8}\ mA \cdot cm^{-2}$; $J_{ph} = 17 mA \cdot cm^{-2}$; $R_{SH} = 600\,\Omega.cm^2$; $\eta = 1.5$)

Three-dimensional modeling of the effect of series resistance on the J(V) characteristic

Figures 7 illustrate in three dimension representations the evolution of the current density versus the bias voltage and the series resistance J(V, R_S, R_{SH} = 600 Ω.cm^2). We remark that the behavior of the current density for the different values of R_S (0 Ω.cm^2 to 30 Ω.cm^2) is similar. This is explained by the fact that the series resistance does not influence the open-circuit voltage V_{oc} and slightly affects the short-circuit current J_{sc} for values of R_S ranging between 0 Ω.cm^2 and 30 Ω.cm^2 with R_{SH} fixed at 600 Ω.cm^2.

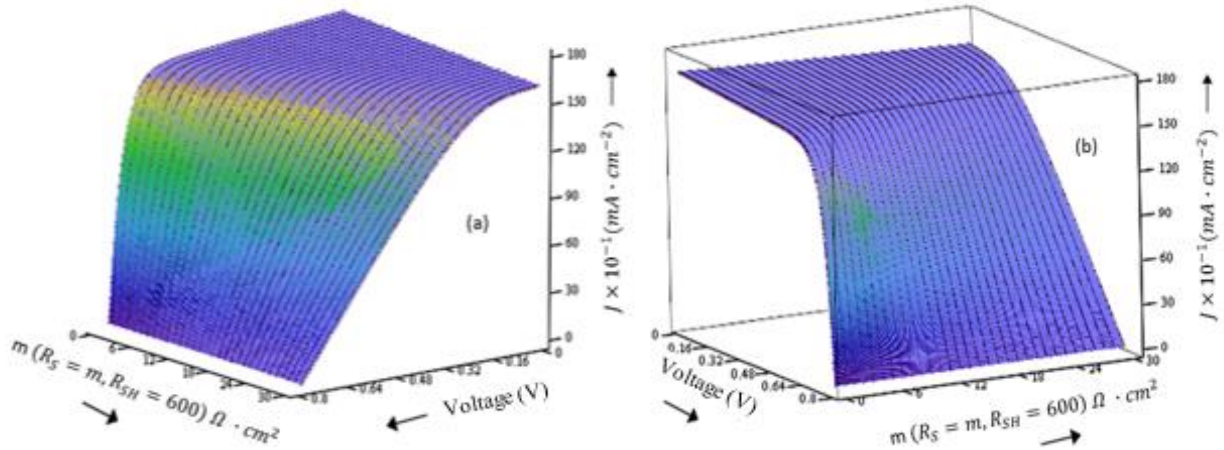

Figure 7: Three-dimensional representation of current density versus bias voltage V and series resistance $R_S\ (R_S = 0\ \Omega.cm^2\ to\ 30\ \Omega.cm^2)$

Figures (a) and (b) are identical only the angles of view differ

$(J_0 = 4.117 \cdot 10^{-8}\ mA \cdot cm^{-2};\ J_{ph} = 17mA \cdot cm^{-2};\ R_{SH} = 600\ \Omega.cm^2;\ \eta = 1.5)$

Evolution of some parameters according to parasitic resistances

In figures 8, we study the evolutions of the short-circuit current density, the open-circuit voltage, the fill factor and the efficiency versus the series resistance (0 Ω.cm^2<R_S<30 Ω.cm^2) for different values of the shunt resistance (5Ω.cm^2<R_{SH}<500Ω.cm^2). Figure 8-a represents the evolution of the short-circuit current density versus the series resistance for different values of the shunt resistance. We remark that for R_S=0 Ω.cm^2, the short-circuit current J_{sc} is independent of the shunt resistance, it remains equal to 17 mA.cm^{-2}. We also note that J_{sc} decreases versus the series resistance for each fixed value of R_{SH}. This decrease is low when R_{SH}>250 Ω.cm^2 where J_{sc} varies between 17 mA.cm^{-2} and 16 mA.cm^{-2}. Figure 8-b shows the evolution of the open-circuit voltage, it is independent of the series resistance, it depends only on the shunt resistance and increases with the latter. For values of R_{SH}>150 Ω.cm^2, we notice that it becomes independent of the parasitic resistances and is in the order of 0.76 V. Figure 8-c shows the evolution of the fill factor, we notice that it is independent of the parasitic resistances when R_{SH}<30 Ω.cm^2 and is in the order of 0.25. For values of R_{SH}>50 Ω.cm^2 it decreases according to the series resistance. It is in order of 0.76 when R_S=0 Ω.cm^2 and R_{SH}=500 Ω.cm^2. Figure 8-d shows the evolution of the efficiency versus the series resistance (Ω.cm^2<R_S<30 Ω.cm^2) for different values of the shunt resistor (5 Ω.cm^2<R_{SH}<500 Ω.cm^2). We notice that the efficiency of the solar cell decreases according to the series resistance for each fixed value of the shunt resistance. In the case of $ZnO(n^+)/CdS(n)/CuInS_2(p)/CuInSe_2(p^+)$ solar cell, this efficiency is less than 5% for R_{SH}<50 Ω.cm^2, it is in order of 12% for R_S=0 Ω.cm^2 and R_{SH}=500 Ω.cm^2. It varies between 6% and 12% for 150 Ω.cm^2<R_{SH}<500 Ω.cm^2.

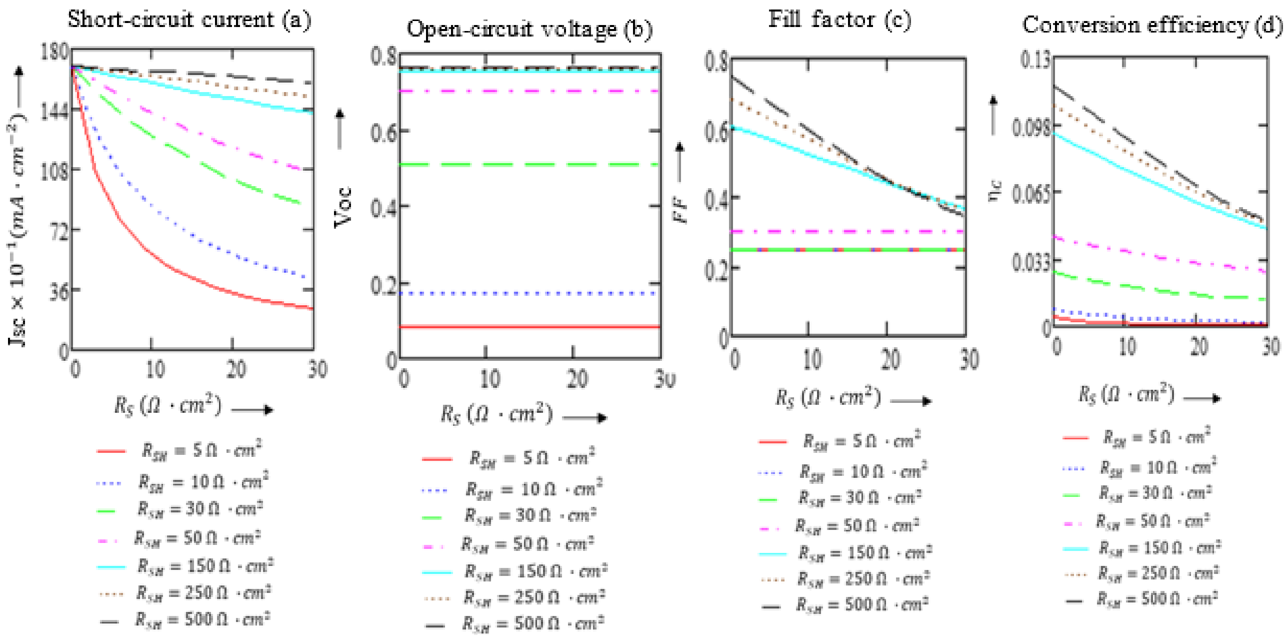

Figure 8: Evolution of some parameters according to the series resistance R_S ($R_S = 0\ \Omega.cm^2$ to $30\ \Omega.cm^2$) for various values of shunt resistance R_{SH} ($R_{SH} = 5\ \Omega.cm^2$ to $500\ \Omega.cm^2$) : a) Short-circuit current density; b) Open circuit voltage; c) Fill factor; d) Electrical power conversion efficiency. ($J_0 = 4.117 \cdot 10^{-8}\ mA \cdot cm^{-2}$; $J_{ph} = 17 mA \cdot cm^{-2}$; $\eta = 1.5$)

Conclusion

The influence of the series resistance on the performance of a solar cell has been essentially developed in this paper. We have established the expressions of the photocurrent due to the illumination and the electrical parameters which characterize a solar cell by considering the single diode model. Then we studied the series resistance effect on the current-voltage characteristic, the power-voltage characteristic and parameters such as the short-circuit current, the open-circuit voltage, the fill factor and the conversion efficiency. The results obtained are applied to the heterostructure based on $CuInS_2$ and $CuInSe_2$ model $ZnO(n^+)/CdS(n)/CuInS_2(p)/CuInSe_2(p^+)$.

The results obtained showed that the series resistance (R_s) does not affect the open-circuit voltage, but it can lead to a decrease of the short-circuit current for its high value (greater than 30 $\Omega.cm^2$). Series resistance effects are manifested by the presence of a slope equal to -1/Rs in the vicinity of the open-circuit voltage, this slope is all the more visible on the current-voltage characteristic as the value of Rs is high. The results obtained showed that an increase of the series resistance decreases the performance, namely the efficiency and the power of the solar cell. In the case of the considered structure $ZnO(n^+)/CdS(n)/CuInS_2(p)/CuInSe_2(p^+)$, depending on the values of the used parameters and by varying the series resistance between 0 $\Omega.cm^2$ and 30 $\Omega.cm^2$, the obtained efficiency varies between 6% and 12% (for shunt resistance greater than 150 $\Omega.cm^2$) under the solar spectrum AM1.5 and the power between 11 $mW.cm^{-2}$ and 4.4 $mW.cm^{-2}$.

Appendix

Determination method of photo- generated current.

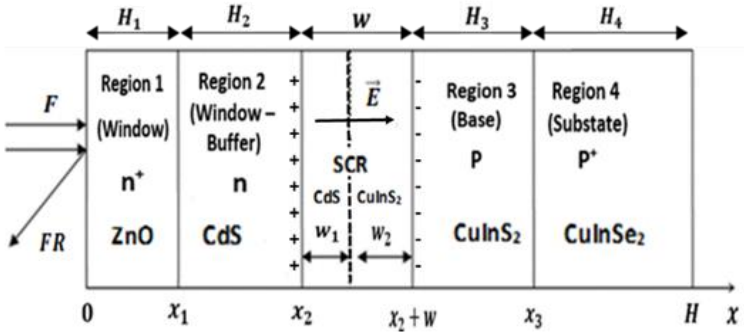

Figure 9: Diagram of the structure $ZnO(n^+)/CdS(n)CuInS_2(p)/CuInSe_2(p^+)$

Continuity equation of minority carriers respectively in region 1 (holes), region 2 (holes), region 3 (electrons), region 4 (electrons) [18-19, 21-23]:

$$\frac{d^2\Delta p_1}{dx^2} - \frac{\Delta p_1}{{L_{p_1}}^2} = \frac{-\alpha_1 F(1-R)e^{-\alpha_1 x}}{D_{p_1}} \quad \text{(A-1)}$$

$$\frac{d^2\Delta p_2}{dx^2} - \frac{\Delta p_2}{{L_{p_2}}^2} = \frac{-\alpha_2 F(1-R)e^{-\alpha_1 H_1}e^{-\alpha_2(x-H_1)}}{D_{p_2}} \quad \text{(A-2)}$$

$$\frac{d^2\Delta n_3}{dx^2} - \frac{\Delta n_3}{L_{n_3}^2} = \frac{-\alpha_3}{D_{n_3}}F(1-R)e^{-\alpha_1 H_1}e^{-\alpha_2(H_2+w_1)}e^{-\alpha_3[x-(H_1+H_2+w_1)]} \quad \text{(A-3)}$$

$$\frac{d^2\Delta n_4}{dx^2} - \frac{\Delta n_4}{L_{n_4}^2} = \frac{-\alpha_4}{D_{n_4}}F(1-R)e^{-\alpha_1 H_1}e^{-\alpha_2(H_2+w_1)}e^{-\alpha_3(H_3+w_2)}e^{-\alpha_4[x-(H-H_4)]} \quad \text{(A-4)}$$

In Region 1 boundary conditions are given by [22, 26]:

$$D_{p_1}\left(\frac{d\Delta p_1}{dx}\right) = S_{p_1}\Delta p_1 \text{ for } x = 0 \quad \text{(A-5)}$$

$$\Delta p_1 = 0 \text{ for } x = x_1 \quad \text{(A-6)}$$

In region 2 boundary conditions are given by [23, 27, 28]:

$$D_{p_2}\frac{d\Delta p_2}{dx} = S_{p_2}\Delta p_2 + D_{p_1}\frac{d\Delta p_1}{dx} \text{ for } x = x_1 \quad \text{(A-7)}$$

$$\Delta p_2 = 0 \text{ for } x = x_2 \quad \text{(A-8)}$$

In region 4 boundary conditions are given by [22, 26]:

$$D_{n_4}\frac{d\Delta n_4}{dx} = -S_{n_4}\Delta n_4 \text{ for } x = H \quad \text{(A-9)}$$

$$\Delta n_4 = 0 \text{ for } x = x_3 \quad \text{(A-10)}$$

In region 3 boundary conditions can be written as [19]:

$$\Delta n_3 = 0 \text{ for } x = x_2 + w \quad \text{(A-11)}$$

$$D_{n_3}\frac{d\Delta n_3}{dx} = -S_{n_3}\Delta n_3 + D_{n_4}\frac{d\Delta n_4}{dx} \text{ for } x = x_3 \quad \text{(A-12)}$$

Photo- generated current due by minority carries [18-19, 21-23]:

$$J_{p_{1-2}} = -qD_{p_2}\left.\frac{d\Delta p_2}{dx}\right|_{x=x_2} \quad \text{(A-13)}$$

$$J_{n_{3-4}} = qD_{n_3}\left.\frac{d\Delta n_3}{dx}\right|_{x=x_2+w} \quad \text{(A-14)}$$

$$J_{SCR} = -qF(1-R)e^{-\alpha_1 H_1}\{e^{-\alpha_2 H_2}\times[e^{-\alpha_2 w_1}-1] + e^{-\alpha_2(H_2+w_1)}\times[e^{-\alpha_3 w_2}-1]\} \quad \text{(A-15)}$$

References

[1]. Safae AAZOU & El Mahdi ASSAID, "Modelling Real Photovoltaic Solar Cell Using Maple", in: International Conference on Microelectronics - ICM, 2009 - ieeexplore.ieee.org DOI: 10.1109/ICM.2009.5418600

[2]. E. Assaid and M. El Aydi, "Exact Analytical Solutions of Diodes Bridge, Maple application center", January 2007. Available online at the electronic address: http://www.maplesoft.com/applications/app_center_ view.aspx?AID=2039.

[3]. E. Assaid, E. Feddi and M. El Aydi, "Exact Analytical Expressions of Graëtz Bridge Currents and Voltages Using LambertW Function", The 14th IEEE International Conference on Electronics, Circuits and Systems, Marrakech, Morocco, december 11-14, 2007.

[4]. A. Orioli, A. D. Gangi, ''A procedure to calculate the five-parameter model of crystalline silicon photovoltaic modules on the basis of the tabular performance data'', Appl Energy 2013;102:1160–77.

[5]. M. R. AlRashidi, M. F. AlHajri, K. M. El-Naggar, A. K. Al-Othman, "A new estimation approach for determining the I–V characteristics of solar cells", Solar Energy 85 (2011) 1543–1550 doi:10.1016/j.solener.2011.04.013.

[6]. W. Xiao, M. G. J. Lind, W. G. Dunford, A., Capel, "Real-time identification of optimal operating points in photovoltaic power systems", IEEE Transactions on Industrial Electronics 53 (4), 1017–1026, 2006.

[7]. B Amrouche, A Guessoum, M Belhamel, "A simple behavioural model for solar module electric characteristics based on the first order system step response for MPPT study and comparison", Appl Energy 2012; 91: 395–404.

[8]. K Ishaque, Z Salam, S Mekhilef, A Shamsudin, "Parameter extraction of solar photovoltaic modules using penalty-based differential evolution", Appl Energy 2012; 99: 297–308.

[9]. Alireza Askarzadeh, Alireza Rezazadeh, "Artificial bee swarm optimization algorithm for parameters identification of solar cell models", Applied Energy 102 (2013) 943–949.

[10]. L Sandrolini, M Artioli, U Reggiani, "Numerical method for the extraction of photovoltaic module double-diode model parameters through cluster analysis". Appl Energy 2010; 87: 442–51.

[11]. R. M. Corless, G. H. Gonnet, DE. G. Hare, D. J. Jeffrey, D. E. Knuth, "On the Lambert W-Function", Adv. Comput. Math, 5 (1996) 329

[12]. Jinlei Ding, Rakesh Radhakrishnan, "A new method to determine the optimum load of a real solar cell using the Lambert W-function", Solar Energy Materials & Solar Cells 92 (2008) 1566–1569.

[13]. Adelmo Ortiz-Conde, Francisco J. Garcı´a Sa´nchez, Juan Muci, "New method to extract the model parameters of solar cells from the explicit analytic solutions of their illuminated I–V characteristics", Solar Energy Materials and Solar Cells 90 (3), 352–361, 2006.

[14]. T. Easwarakhanthan, J. Bottin, I. Bouhouch, C. Boutrit., "Nonlinear minimization algorithm for determining the solar cell parameters with microcomputers", Sol Energy 1986; 4:1–12.

[15]. M. Zagrouba, A. Sellami, M. Bouaïcha, M. Ksouri, ''Identification of PV solar cells and modules parameters using the genetic algorithms: Application to maximum power extraction'', Solar Energy 84 (5) (2010) 860 – 866.

[16]. K. M. El-Naggar, M. R. AlRashidi, M. F. AlHajri, A. K. Al-Othman, "Simulated annealing algorithm for photovoltaic parameters identification", Sol Energy 2012; 86: 266–74.

[17]. H. Wei, J. Cong, X. Lingyun, S. Deyun, "Extracting solar cell model parameters based on chaos particle swarm algorithm", In: International conference on electric information and control engineering (ICEICE); 2011. p. 398–402.

[18]. El Hadji Mamadou Keita, Fallou Mbaye, Abdoul Aziz Correa, Mamadou Dia, Cheikh Sene, Babacar Mbow. Ideal Solar Cell Electrical Parameters and Ideality Factor Effect on the Efficiency. International Journal of Energy and Power Engineering. Vol. 12, No. 1, 2023, pp. 9-21. doi: 10.11648/j.ijepe.20231201.12

[19]. E.M. Keita, F. Mbaye, M. Dia, C. Sow, C. Sene, B. Mbow, OAJ Materials and Devices, Vol 7, 0106 - 1 (2023) – DOI: 10.23647/ca.md20230106

[20]. Michelle Schatzman, Cours et Exercices, Analyse Numérique, ''Une Approche Mathématique'', 2001, 2e édition, DUNOD, p.211.

[21]. E. M. Keita, B. Ndiaye, M. Dia, Y. Tabar, C. Sene, B. Mbow,"Theoretical Study of Spectral Responses of Heterojunctions Based on CuInSe2 and CuInS2" OAJ Materials and Devices, Vol 5#1, 0508 (2020) – DOI: 10.23647/ca.md20200508.

[22]. E.M. Keita, Y. Tabar, M.S. Mane, M. Dia, C. Sene, B. Mbow, '' Behavior Study of Heterojunction Based on CuInS2/CuInSe2Solar Cell in Two and Three Dimensional Representations under Monochromatic Light Illumination from Near Infrared to Visible: n+n/pp+ Model'', Journal of Scientific and Engineering Research, 2021, 8(10):106-116

[23]. El Hadji Mamadou Keita, Fallou Mbaye, Bachirou Ndiaye, Chamsdine Sow, Cheikh Sene, Babacar Mbow. Optimizing Structures Based on Chalcopyrite Materials for Photovoltaic Applications. American Journal of Energy Engineering. Vol. 10, No. 3, 2022, pp. 53-67.doi: 10.11648/j.ajee.20221003.11

[24]. Alain Ricaud, "Photopiles Solaires", de la physique de la conversion photovoltaïque aux filières, matériaux et procédés. 1997, 1e édition, Presses polytechniques et universitaires romandes, p. 40.

[25]. R. Scheer, T. Walter, H.W. Schock, M.L. Fearheiley, H.J. Lewerenz,''$CuInS_2$ based thin film solar cell with 10.2% efficiency'', Appl. Phys. Lett. 63 (1993) 3294.

[26]. B. Mbow, A. Mezerreg, N. Rezzoug, and C. Llinares, ''Calculated and Measured Spectral Responses in Near-Infrared of III-V Photodetectors Based on Ga, In, and Sb'', phys. Stat. Sol. (a) 141, 511 (1994).

[27]. H. J. Hovel and J. M. Woodall,'' Ga1-xAlxAs - GaAs P-P-N Heterojunction Solar Cells'', J. Electrochem. Soc. 120, 1246 (1973).

[28]. H. J. Hovel and J. M. Woodall, 10th IEEE Photovoltaic Specialists Conf., Palo Alto (Calif.) 1973 (p.25).